Nanofluidic Diode for Simple Fluids without Moving Parts

Long Li, Jingwen Mo, and Zhigang Li*
Department of Mechanical and Aerospace Engineering, The Hong Kong University of Science and Technology, Clear Water Bay, Kowloon, Hong Kong
(Received 24 July 2015; published 24 September 2015)

The fabrication of small scale, fixed structure fluidic diodes for simple fluids is quite challenging and has not yet been achieved. Here, we fabricate a moving part-free nanofluidic diode for simple fluids using heterogeneous nanochannels, half of which is hydrophilic and the other half is hydrophobic. It accepts water flows in the forward (from hydrophilic to hydrophobic) direction, while the flows in the backward direction are blocked for pressure drop range $0 < \Delta P < 0.63$ MPa. The diode is ensured by a potential energy barrier at the channel entrance on the hydrophobic side due to the molecular interactions between the water and channel surface. As the upstream pressure becomes higher than 0.63 MPa, the fluidic diode turns to be a rectifier, which allows flows in both the forward and backward directions but with different flow rates. At sufficiently high driving pressures, the fluidic system fails in flow rectification, analogous to the breakdown of electronic diodes. The three different flow modes (diode, rectifier, and breakdown) of the fluidic chip and the underlying rectification mechanisms are confirmed by molecular dynamics simulations.

DOI: 10.1103/PhysRevLett.115.134503 PACS numbers: 47.61.Fg, 85.85.+j

Fluid flow regulations at micro- and nanoscales are essential in integrated fluidic devices and micro total analysis systems, which have tremendous applications in biology, medicine, chemistry, and engineering [1–4]. Analogous to electronic diodes, fluidic diodes are expected to generate unidirectional flows and appear to be efficient components for flow controls. Microvalves can act as fluidic diodes. However, they usually contain moving parts, which cause reliability issues at small scales and require external actuations to provide driving forces [5,6]. These disadvantages place microvalves in an awkward position for microscopic flow manipulations. Small scale fluidic diodes without moving parts, if they could be fabricated, would significantly advance micro- and nanofluidic technologies and their applications in a variety of areas.

Fluid transport is fundamentally different from that of electrons and the fluidity property of fluids makes it difficult to completely prohibit flows in a specific direction in fixed structures. The fabrication of moving part-free fluidic diodes is more challenging than that of electronic diodes. The term "nanofluidic diode" has been used for the rectification of ion transport, which was reached by asymmetric pore geometries and/or surface charge distributions [7–11]. For simple fluids, passive fluidic diodes (no moving parts) have not been fabricated. Practically, the next best choice perhaps is fluidic rectifiers, which allow flows in both the forward and backward directions but favor fluid flows in a particular (say, forward) direction. Fixed structure fluidic rectifiers have been fabricated in the literature [4,12–14]. To achieve flow rectifications, asymmetric structures were employed to generate anisotropic flow resistances in different directions [4,6,12–14]. Theoretically, the direction dependent flow resistance originates from the nonlinear inertial term in the equations of motion (Navier-Stokes equations [15]) for the fluid. Therefore, flow rectifications can only be achieved either by using the nonlinear properties of non-Newtonian fluids (e.g., viscoelastic fluids) or at high Reynolds number ($\mathrm{Re} = \rho V L/\mu$, where ρ, V, and μ are the fluid density, velocity, and viscosity, and L is the characteristic length of the flow system) [4,13,16]. Nonetheless, even if these conditions are met, the performance of the existing passive fluidic rectifiers is far from being satisfactory. The diodicity (flow rate or pressure drop ratio between the forward and backward directions) of the available passive rectifiers is usually less than 3 [13]. The poor performance is caused by the difficulty of generating notable anisotropy in flow resistance using fixed structures. For simple fluids and at small scales, Re is very small and the nonlinear fluid properties are negligible. In this case, flow rectifications in passive rectifiers are barely observed. This is why the fabrication of passive fluidic rectifiers is challenging and fluidic diodes without moving parts are unavailable for simple fluids.

An effective approach to achieve flow rectifications or block fluid flows in a specific direction is to develop direction dependent energy barriers for fluid flows. This can be fulfilled in nanochannels by taking advantage of molecular interactions, as inspired by our recent work on fluid infiltration in nanopores [17]. Here, we fabricate a fluidic diode without moving parts using nanochannels of heterogeneous surface energies such that one part of the channel is hydrophilic and the other part is hydrophobic,

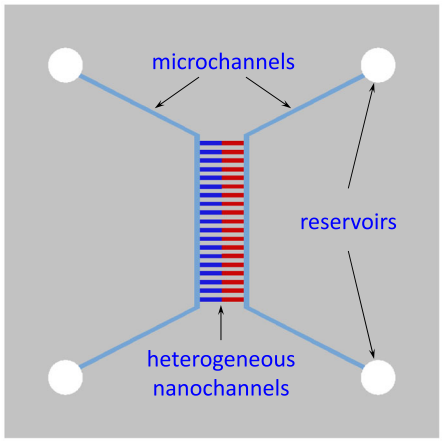

FIG. 1 (color online). Schematic of the nanofluidic system.

which have distinct potential energy barriers at the entrances and require different infiltration pressures. Experiments show that a fluidic diode is achieved with a wide range of pressure drops, $0 < \Delta P < 0.63$ MPa. For pressure drops higher than 0.63 MPa, the diode reduces to a fluidic rectifier, which fails in flow rectification when $\Delta P > 3$ MPa. Molecular dynamics simulations are performed to illustrate the mechanisms and confirm the experimental observations.

The fluidic chip consisted of an array of 200 parallel heterogeneous nanochannels. The left half of the channels was hydrophilic and the right half was hydrophobic. Two microchannels with four fluid reservoirs at the ends connected perpendicularly with the nanochannels to form a nanofluidic system, as illustrated in Fig. 1. The heterogeneous surface properties for the nanochannels were achieved by using the sacrificial machining method [18]. The fabrication of the fluidic chip is illustrated in Fig. 2 (more information can be found in the Supplemental Material [19]). The water contact angles for the hydrophilic and hydrophobic parts were 16° and 158°, respectively, as shown in Fig. S1 (Supplemental Material [19]). The dimensions of the nanochannels were defined as 100 nm, 10 μm, and 200 μm in height, width, and length, respectively. The height and width of the two microchannels were 10 and 50 μm. The top panel of Fig. 3 shows the cross section of a nanochannel under a scanning electron microscopy (SEM), where the height and width of the nanochannel were 97.8 nm and 10 μm.

The experimental setup is depicted in Fig. 4 (details can be found in the Supplemental Material [19]). A syringe pump was used to generate a desired flow rate of deionized (DI) water with an accuracy of 0.001 μl/h. The pressures of the reservoirs P_1 to P_4 were measured by pressure transducers, as shown in Fig. 4. As the flow resistance in nanochannels is much larger than that in microchannels [24–26], the pressure drop ΔP over the nanochannels could be calculated as that between the upstream and downstream

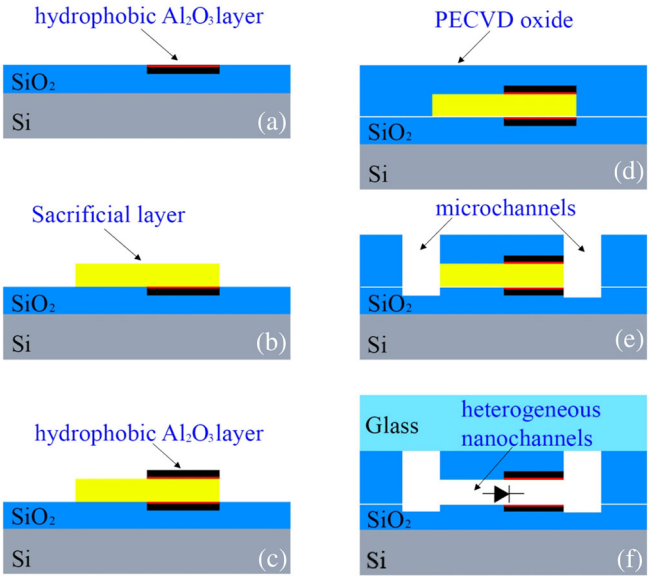

FIG. 2 (color online). Fabrication process for the nanofluidic chip (dimensions are not in scale). (a) Growth of 5-nm-thick Al_2O_3 layer on SiO_2-coated silicon wafer through photolithography and wet etching. The Al_2O_3 layer was subsequently modified by low surface energy material (red). (b) Deposition of silicon sacrificial layer. (c) Fabrication of another Al_2O_3 layer serving as the top wall of the hydrophobic part. (d) Wrapping with SiO_2 layer through plasma-enhanced chemical vapor deposition. (e) Reactive ion etching of microchannels and reservoirs (not shown). (f) Anodic bonding of glass cover and removal of sacrificial layer.

reservoirs (e.g., $\Delta P = P_1 - P_3$ for forward flows, from hydrophilic to hydrophobic side). Valves were used to regulate flows and remove air from the system before experiments. The fluidic chip was tested by fluorescent dye (Rhodamine 6 G)-laden DI water. A snapshot of a forward

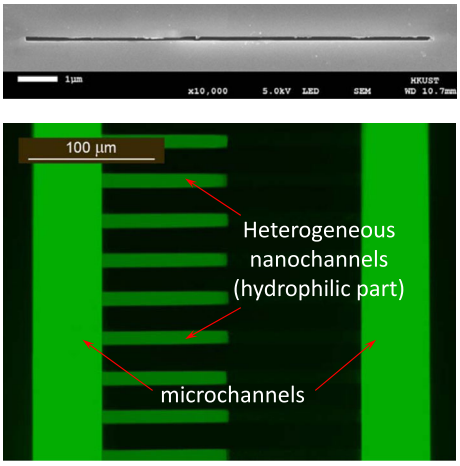

FIG. 3 (color online). Nanochannel characterization. Top panel: SEM image showing the height (97.8 nm) and width (10 μm) of a nanochannel. Bottom panel: microscopic image of a fluorescent flow through the fluidic chip.

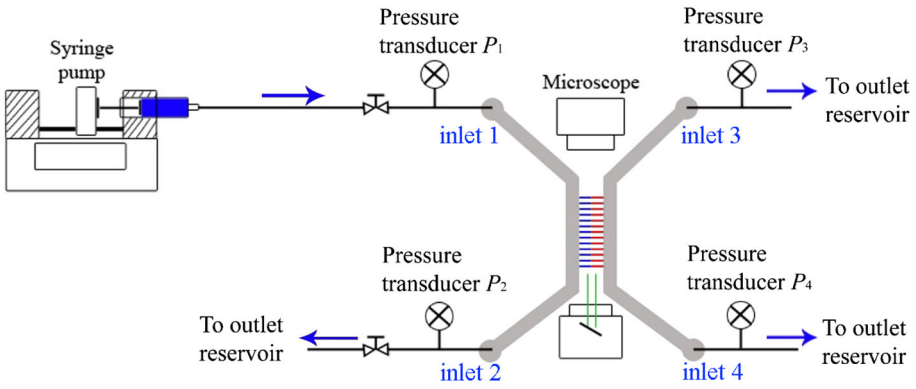

FIG. 4 (color online). Experimental setup of the fluidic system. DI water is driven by a syringe pump with a desired flow rate. Arrows indicate the directions of forward flows. Pressures of the reservoirs $P_1 - P_4$ are measures by pressure transducers.

flow is displayed in Fig. 3 (bottom panel). It is seen that the flow (green) could go through nanochannels smoothly from the left to the right microchannel, indicating that the nanochannels were free of collapse (the hydrophobic part was not transparent to fluorescence).

DI water was pumped through the heterogeneous channels with different flow rates in both the forward (inlet 1 → inlet 3) and backward (inlet 3 → inlet 1) directions (Fig. 4). The valves connecting inlets 2 and 4 were turned off after the removal of air and the downstream inlet was open to atmosphere. Figure 5 plots the total volumetric flow rate Q and flux as a function of ΔP. In both directions, the flow rates in each channel were always lower than the predictions of the classic Navier-Stokes equations $Q_{\mathrm{NS}} = h^3 w \Delta P/(12\ \mu l)$, where h, w, and l are the channel height, width, and length, respectively. This is caused by the large flow resistance at the nanoscale [24,25,27]. In the forward direction, it is seen that Q kept increasing as the pressure drop was raised. At low pressure drops, Q showed a faster-than-linear dependence on ΔP due to the flow slip at the interface [15,28,29]. After that, Q increased gently. This might be caused by the large friction due to the enhanced molecular interactions at the interface at high pressures [30,31]. Another reason for the nonlinear dependence could be the nonuniform surface properties, which generate complex potential distributions at the center part of the channels, as will be shown later. In the backward direction, the flow rate was lower than that in the forward direction though it followed a similar fashion. In addition, the flow was blocked when the pressure drop was lower than 0.63 MPa, as shown in Fig. 5. This indicates that the fluidic system served as a fluidic diode for $\Delta P < 0.63$ MPa. For $0.63 < \Delta P < 3$ MPa, it behaved as a fluidic rectifier, which allows fluid flows in both directions but with different flow rates. The diodicity is shown in the inset of Fig. 5 as a function of flow rate Q. The largest diodicity was about 6, which is the highest ever for fluidic rectifiers [4,13]. As the pressure drop went higher, the flow rates in both directions became approximately the same and flow rectifications could not be reached, similar to the breakdown of electronic diodes.

Therefore, the heterogeneous nanochannel fluidic system experienced three modes, i.e., fluidic diode, rectifier, and breakdown, as the pressure drop was increased. If the flow rate is expressed as $Q = \Delta P/R$, where R is the flow resistance, the flow rectifications observed must be caused by different flow resistances in the two directions. In macroscale fluidic systems, the flow resistance in uniform-sized channels is mainly caused by the shearing stress at the fluid-wall interface, which remains the same regardless of the flow direction. At the nanoscale, the flow resistance inside a channel R_{ch} is also independent of flow directions. However, the molecular interactions between water molecules and wall atoms become dominant in nanochannels and develop a potential energy barrier at the entrance if the channel is of low surface energy (i.e., hydrophobic channel) [17]. For hydrophilic channels (high

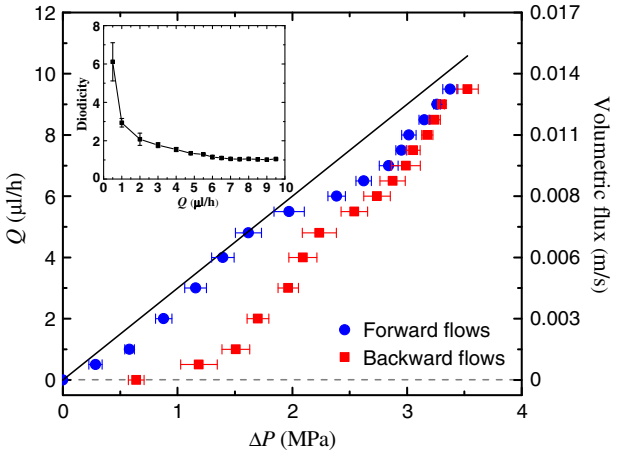

FIG. 5 (color online). Total volumetric flow rate and flux through the fluidic chip as a function of ΔP. The solid line is the prediction of the Navier-Stokes equations. Error bars denote the standard deviation of three experiments. Diodicity in the inset represents the pressure drop ratio between the forward and backward directions.

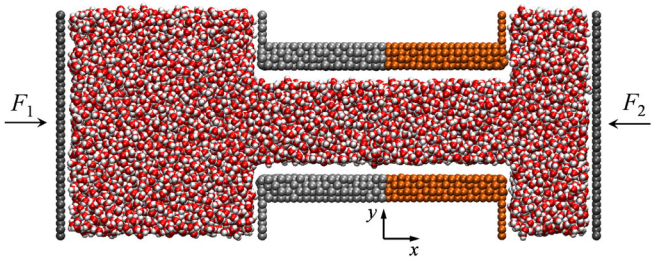

FIG. 6 (color online). A snapshot of the molecular dynamics simulation system. The left and right halves of the channel are hydrophilic and hydrophobic.

surface energy), the water-wall attractive force is strong and can facilitate the infiltration of water, leading to capillarity. Hence, for the heterogeneous nanochannel fluidic system, the energy barrier at the hydrophobic entrance introduces extra flow resistance R_{en} in the backward direction, which requires the upstream pressure P_{up} to reach a critical value P^* to drive water through the channel. If $P_{up} < P^*$, flows in the backward direction are prohibited and the fluidic system works as a diode. If P_{up} is higher than P^*, flows in both directions become possible but the anisotropic flow resistances make the flow rate in the forward direction $Q_F = \Delta P/R_{ch}$ different from that in the backward $Q_B = \Delta P/(R_{en} + R_{ch})$ direction. When P_{up} is sufficiently high such that $P_{up} \gg P^*$, the entrance energy barrier plays a minor role and the flow rectification disappears (breakdown).

To confirm the experiments and rectification mechanisms, molecular dynamics (MD) simulations are conducted to study water flows in nanochannels. The MD system consists of a 3.3-nm-high heterogeneous nanochannel and two fluid reservoirs, as shown in Fig. 6 (details can be found in the Supplemental Material [19] and Refs. [17] and [32]). Flows are generated by two rigid pistons (Fig. 6), on which constant forces are applied to control the pressure of the reservoirs. The temperature of the system is maintained at 300 K by the Berendsen thermostat [33]. The heterogeneous surfaces are realized by changing the water-surface binding energy ε_{ws} [32], which is 300 and 50 K for the hydrophilic and hydrophobic parts, respectively. The corresponding water contact angles are 27° and 131° [17].

First, we compute the potential energy in the channel. The contour plot of the potential distribution next to the bottom surface in an x-y plane is illustrated in Fig. 7. It is seen that the potential energy is greatly affected by the surface properties, especially at the entrances near the channel surface. The average potential energies at the entrances on the hydrophilic and hydrophobic sides in the plane in Fig. 7 are −0.023 and −0.003 eV, respectively. It is also seen that the potential difference between the two entrances grows larger as a water molecule approaches the channel surface, as shown in the inset of Fig. 7. Since the average kinetic and potential energies of water molecules at room temperature are around 0.1 and −0.4 eV [16], water

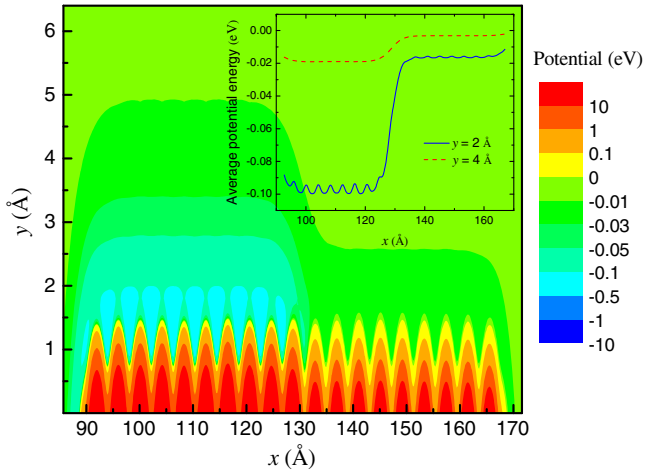

FIG. 7 (color online). Potential energy distribution in an x-y plane near the bottom surface ($y = 0$) of the nanochannel in MD simulations. The hydrophilic and hydrophobic entrances are at $x = 90$ and 168 Å, respectively. The inset shows the potential energies along $y = 2$ and 4 Å.

molecules will have difficulty in transporting to areas of potential energy higher than −0.3 eV without the assist of external forces. Therefore, the entrance potential at the hydrophobic side sets an energy barrier (Fig. 7), which requires a relatively high pressure to help water molecules infiltrate into the channel.

Figure 8 depicts the volumetric flux obtained in MD simulations as a function of pressure difference between the reservoirs ΔP. For $\Delta P < 3$ MPa, the flow from the hydrophobic to hydrophilic side is blocked and the heterogeneous nanochannel acts as a diode. This pressure drop window for the system to be a diode is larger than that in the experiments (Fig. 5) because the channel size in the MD simulation is small and surface effects are significant. As

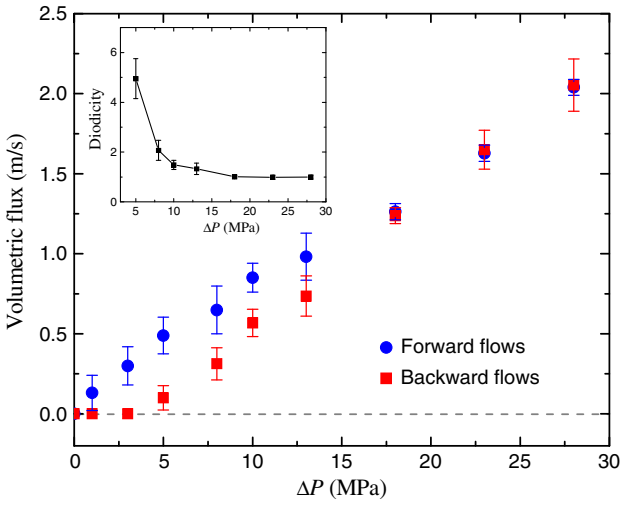

FIG. 8 (color online). Volumetric flux obtained in the MD simulations. Diodicity in the inset denotes the flux ratio.

the pressure drop is increased, water flows in both directions are observed and the system changes to a flow rectifier. For $\Delta P > 18$ MPa, the flow rates in both directions become the same, which is the breakdown of the diode or rectifier. Therefore, the MD results for the three different flow modes are consistent with the experiments in Fig. 5. It is noted that the critical pressure P^* depends on the surface energy of the hydrophobic part and channel size [17]. If the surface energy or channel size is reduced, the entrance energy barrier at the hydrophobic side will increase, which will lead to a high P^*. Molecular dynamics simulations (not reported here) in a 5-nm-high channel with the same surface energy as that in Fig. 8 show that $P^* = 2.5$ MPa, which is lower than that (3 MPa) in Fig. 8. It is also worth mentioning that membranes with different surface properties have been fabricated, which showed diodelike permeability for water [34]. However, the pore size of the membranes was at microscale, where the entrance energy barrier was insignificant. Therefore, the flow modes observed in our work may not occur there.

In summary, we have fabricated a nanofluidic system using heterogeneous nanochannels. Because of asymmetric flow resistances caused by the entrance energy barrier, the fluidic system worked as a fluidic diode for a wide range of pressure drops. It turned to be a flow rectifier as the upstream pressure became higher than the critical pressure required to overcome the entrance energy barrier. The breakdown of the diode or rectifier was observed when the driving pressure was sufficiently higher than the critical pressure. Molecular dynamics simulations confirmed the flow modes in experiments and the explanation about the anisotropic flow resistances due to the potential energy barrier at the hydrophobic entrance.

This work was supported by the Research Grants Council of the Hong Kong Special Administrative Region under Grant No. 16205714. J. M. was partially supported by the Energy Program at HKUST. We thank the Nanoelectronics Fabrication Facility at the Hong Kong University of Science and Technology for the device fabrication.

L. L. and J. M. contributed equally to this work.

*mezli@ust.hk

[1] T. Thorsen, S. J. Maerkl, and S. R. Quake, Science **298**, 580 (2002).
[2] D. Mark, S. Haeberle, G. Roth, F. von Stetten, and R. Zengerle, Chem. Soc. Rev. **39**, 1153 (2010).
[3] P. S. Dittrich and A. Manz, Nat. Rev. Drug Discov. **5**, 210 (2006).
[4] A. Groisman and S. R. Quake, Phys. Rev. Lett. **92**, 094501 (2004).
[5] K. W. Oh and C. H. Ahn, J. Micromech. Microeng. **16**, R13 (2006).
[6] M. Nabavi, Microfluid. Nanofluid. **7**, 599 (2009).
[7] A. Alcaraz, P. Ramirez, E. Garcia-Gimenez, M. L. Lopez, A. Andrio, and V. M. Aguilella, J. Phys. Chem. B **110**, 21205 (2006).
[8] R. Karnik, C. H. Duan, K. Castelino, H. Daiguji, and A. Majumdar, Nano Lett. **7**, 547 (2007).
[9] V. Z. S. Siwy, Nano Lett. **7**, 552 (2007).
[10] S. Wu, F. Wildhaber, A. Bertsch, J. Brugger, and P. Renaud, Appl. Phys. Lett. **102**, 213108 (2013).
[11] Y. Kong, X. Fan, M. H. Zhang, X. Hou, Z. Y. Liu, J. Zhai, and L. Jiang, ACS Appl. Mater. Interfaces **5**, 7931 (2013).
[12] N. Tesla, Valvular Conduit, U.S. Patent No. 1329559 (1920).
[13] P. C. Sousa, F. T. Pinho, M. S. N. Oliveira, and M. A. Alves, J. Non-Newtonian Fluid Mech. **165**, 652 (2010).
[14] J. Su, K. Yang, and H. Guo, R. Soc. Chem. Adv. **4**, 40193 (2014).
[15] B. R. Munson, D. F. Young, and T. H. Okiishi, *Fundamentals of Fluid Mechanics* (Wiley & Sons, Singapore, 2006).
[16] N. T. Nguyen, Y. C. Lam, S. S. Ho, and C. L. N. Low, Biomicrofluidics **2**, 034101 (2008).
[17] J. W. Mo, L. Li, J. F. Zhou, D. Y. Xu, B. L. Huang, and Z. G. Li, Phys. Rev. E **91**, 033022 (2015).
[18] J. Cheng and L. J. Guo, ACS Nano **3**, 575 (2009).
[19] See Supplemental Material at http://link.aps.org/supplemental/10.1103/PhysRevLett.115.134503 for chip fabrication, flow characterization, and MD simulations, which includes Refs. [20–23].
[20] F. Cleri and V. Rosato, Phys. Rev. B **48**, 22 (1993).
[21] Z. Li and H. Wang, Phys. Rev. Lett. **95**, 014502 (2005).
[22] H. J. C. Berendsen, J. R. Grigera, and T. P. Straatsma, J. Phys. Chem. **91**, 6269 (1987).
[23] Z. G. Li, Phys. Rev. E **80**, 061204 (2009).
[24] C. Liu and Z. G. Li, Phys. Rev. E **80**, 036302 (2009).
[25] C. Liu and Z. G. Li, AIP Adv. **1**, 032108 (2011).
[26] L. Li, J. W. Mo, and Z. G. Li, Phys. Rev. E **90**, 033003 (2014).
[27] Q. Wu, J. T. Ok, Y. Sun, S. T. Retterer, K. B. Neeves, X. Yin, B. Bai, and Y. Ma, Lab Chip **13**, 1165 (2013).
[28] Y. Zhu and S. Granick, Phys. Rev. Lett. **87**, 096105 (2001).
[29] S. Lichter, A. Roxin, and S. Mandre, Phys. Rev. Lett. **93**, 086001 (2004).
[30] Z. G. Li, Phys. Rev. E **79**, 026312 (2009).
[31] C. Liu and Z. G. Li, J. Chem. Phys. **132**, 024507 (2010).
[32] C. Liu and Z. G. Li, Phys. Rev. Lett. **105**, 174501 (2010).
[33] Allen D. Tildesley, *Computer Simulation of Liquids* (Oxford University Press, New York, 1987).
[34] E. Bormashenko, S. Balter, A. Malkin, and D. Aurbach, Macromol. Mater. Eng. **299**, 27 (2014).